High-pressure optical study of small-diameter chirality-enriched single-wall carbon nanotubes

Markus Krottenmüller, W. Gao, Badawi Anis, J. Kono, Christine A. Kuntscher

Angaben zur Veröffentlichung / Publication details:

Krottenmüller, Markus, W. Gao, Badawi Anis, J. Kono, and Christine A. Kuntscher. 2016. "High-pressure optical study of small-diameter chirality-enriched single-wall carbon nanotubes." *physica status solidi (b)* 253 (12): 2446–50. https://doi.org/10.1002/pssb.201600358.

High-pressure optical study of small-diameter chirality-enriched single-wall carbon nanotubes

M. Krottenmüller[1], W. Gao[2], B. Anis[3], J. Kono[2], and C. A. Kuntscher[*,1]

[1] Experimentalphysik 2, Universität Augsburg, 86159 Augsburg, Germany
[2] Department of Electrical and Computer Engineering, Department of Physics and Astronomy, and Department of Materials Science and NanoEngineering, Rice University, Houston, Texas 77005, USA
[3] Spectroscopy Department, Physics Division, National Research Centre, 33 El Bohouth st. (former El Tahrir st.), P. O. 12622, Dokki, Giza, Egypt

[*] Corresponding author: e-mail christine.kuntscher@physik.uni-augsburg.de, Phone: +49-(0)821 598 3315, Fax: +49-(0)821 598 3411

1 Introduction Carbon nanotubes are cylindrical nanostructures conceptually obtained by rolling up a sheet of graphene. Single-wall carbon nanotubes (SWCNTs) exhibit unique optical, electronic, and mechanical properties. Their robust mechanical properties are due to the strong conjugated covalent bonds between the sp^2 orbitals of the carbon atoms resulting from the close relation to graphene [1]. Their mechanical stability has been extensively investigated under high external pressure, usually via x-ray diffraction [2, 3] and Raman spectroscopy [4–8]. Recently, optical spectroscopy studies on SWCNTs under high pressure [9–11] revealed a complementary method for investigating the mechanical stability and structural transitions under pressure of SWCNTs by probing their electronic properties. It has been shown that the filling of SWCNTs with inner tubes leads to a stabilization of the outer tubes [12–14]. The higher mechanical stability is due to the smaller diameter of the inner tubes, and this finding is in accordance to theoretical investigations [15–17], which find the critical pressure for a structural phase transition of SWCNTs scaling with the nanotube diameter according to d^{-3}.

Depending on the direction of rolling up the graphene sheet, SWCNTs appear in different chiralities described by the chiral indices n,m [1]. In any common growth method, SWCNT samples are produced containing many different chiralities. Since electronic properties of SWCNTs highly depend on the chirality [18], the presence of various chiralities leads to inhomogeneous broadening of electronic transitions because the different contributions cannot be resolved. Therefore, much effort has been put in the preparation of chirality-enriched SWCNT samples [19]. With methods such as density gradient ultracentrifugation [20], gel chromatography [21], DNA-wrapping [22], or direct chirality-specific growth on solid alloy catalysts [23] one is capable of preparing macroscopic ensembles of SWCNTs of specific chiralities. However, all these methods suffer from high costs and low yield. Aqueous two-phase extraction [24] is an alternative rapid method to obtain high-purity

SWCNTs of almost any species without the need of high-cost equipment.

Here, we present a high-pressure optical spectroscopy study of a (6,5)-enriched SWCNT film. The sample was first characterized by optical spectroscopy under ambient conditions. Optical absorbance spectra were then measured under pressure up to 22 GPa at room temperature. We found a critical pressure, corresponding to a structural phase transition of (6,5) SWCNTs, which is higher than that for SWCNTs with 1.4 nm average diameter, confirming the expected higher mechanical stability of small-diameter SWCNTs.

2 Experimental We first prepared a suspension of (6,5) chirality-enriched SWCNTs (CE-SWCNTs) using the aqueous two-phase extraction (ATPE) method starting from well-defined CoMoCAT SWCNTs (SG65i, Southwest Nanotechnologies, diameter: 0.7–0.9 nm, (6,5) content >40%), as described in Ref. [24]. Then, we used vacuum filtration to prepare a film with a thickness of ≈100 nm [25]. A detailed characterization of (6,5)-ATPE sorted CoMoCAT SWCNTs by Raman, photoluminescence, and optical absorption spectroscopy can be found in Refs. [24, 25]. For comparison, a similar film of chirality-mixed SWCNTs (CM-SWCNTs) (arc-discharge SWCNTs Type P2 from Carbon Solutions, Inc.) with an average diameter of 1.4 nm on top of a cellulose nitrate membrane was prepared from a Triton X-100 suspension [26]. Free-standing films of the two samples were obtained by removing the polycarbonate and cellulose nitrate membranes with chloroform and acetone, respectively. Because of strong ultrasonication using a tip sonicator for 1 h during the preparation, both SWCNT samples are assumed to be cap opened [27]. Therefore, both samples will be filled with the pressure transmitting medium during the pressure experiments [8].

Transmission measurements were performed at room temperature at ambient and high pressure. The spectra of the free-standing SWCNT films were recorded in a frequency range of 2500–22000 cm^{-1} with a resolution of 4 cm^{-1}, using a Bruker IFS 66v/S Fourier transform infrared spectrometer in combination with an infrared microscope (Bruker IR Scope II) with a 15× Cassegrain objective. A Syassen–Holzapfel [28] diamond anvil cell (DAC) was used to generate high pressure, which was determined *in situ* by the ruby luminescence technique [29]. Liquid nitrogen was used as the pressure transmitting medium (PTM), since it provides hydrostatic conditions up to high pressure [30]. The intensity of the radiation transmitted through the sample, I_s, and the intensity of the radiation transmitted through the PTM in the DAC, I_{ref}, were measured *in situ*. The transmittance $T(\omega)$ and absorbance $A(\omega)$ spectra were calculated according to $T(\omega) = I_s(\omega)/I_{ref}(\omega)$ and $A(\omega) = -\log_{10} T(\omega)$, respectively. The measurement geometry is illustrated in Fig. 1 of Ref. [9] where the sample was swimming freely in the PTM.

3 Results and discussion

3.1 Characterization of a free-standing (6,5)-chirality-enriched SWCNT film To verify the chirality enrichment, we firstly characterized the SWCNT films at ambient pressure using optical absorption spectroscopy. The absorbance spectra in the near-infrared and visible (NIR-VIS) frequency range for the (6,5)-ATPE sorted (CE-SWCNTs), the CoMoCAT starting material and the arc-grown chirality-mixed (CM-SWCNTs) samples are plotted in Fig. 1. The CM-SWCNT sample shows several absorption bands corresponding to the S_{11}, S_{22}, and M_{11} optical transitions of SWCNTs as pointed out in the graph. Here, S_{ii} indicates the i-th interband optical transition in semiconducting tubes, while M_{11} stands for the first interband optical transition in metallic tubes. All the optical transitions exhibit a fine structure, which reflects the nanotube diameter distribution in the CM-SWCNT sample. The CoMoCAT and the CE-SWCNT samples show only the S_{11} and S_{22} optical transitions, as expected, which are shifted to higher frequencies compared to the CM-SWCNT sample due to their smaller diameter [31]. Following the empirical Kataura plot [32, 18], we identify the sharp peaks at 9935 and 17360 cm^{-1} as the S_{11} and S_{22} optical transitions of (6,5) SWCNTs, respectively. The shoulders of the CE-SWCNT sample can be assigned to the S_{11} and S_{22} optical transitions of (9,1) and (7,3) SWCNTs [18], respectively, which are still present in the sample [24, 25]. It is also evident that the features in the CE-SWCNT sample (FWHM of S_{11} transition: 635 cm^{-1}) are much sharper than in the CoMoCAT sample (FWHM of S_{11} transition: 1075 cm^{-1}). This demonstrates the further enrichment of (6,5) species (which is already dominant in CoMoCAT SWCNTs) due to the ATPE sorting.

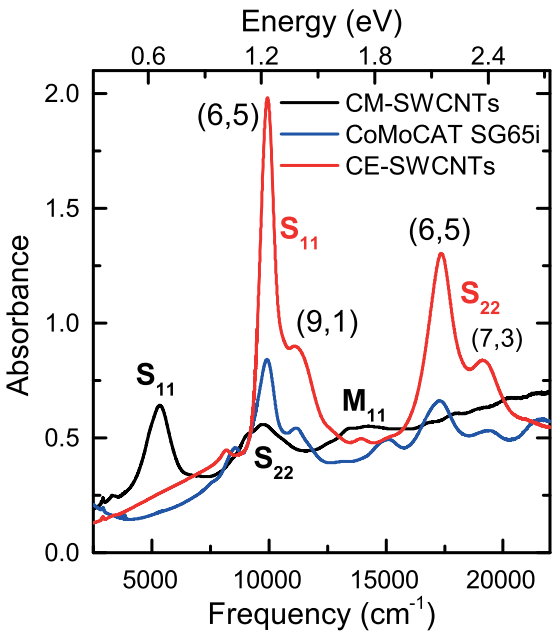

Figure 1 Free-standing NIR-VIS spectra at ambient conditions of the (6,5)-chirality-enriched SWCNT (CE-SWCNT) film in comparison with the films of the CoMoCAT starting material and chirality-mixed SWCNTs (CM-SWCNT) with average diameter of 1.4 nm.

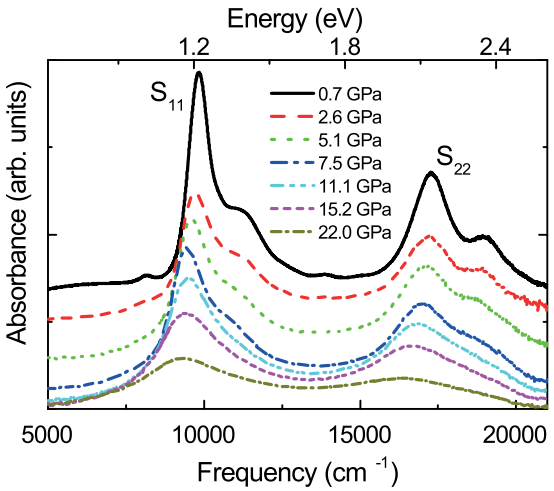

Figure 2 Background-subtracted optical absorbance spectra of the (6,5)-chirality-enriched SWCNT film for various pressures. The first and second optical transitions in the semiconducting (6,5) SWCNTs are marked by S_{11} and S_{22}, respectively.

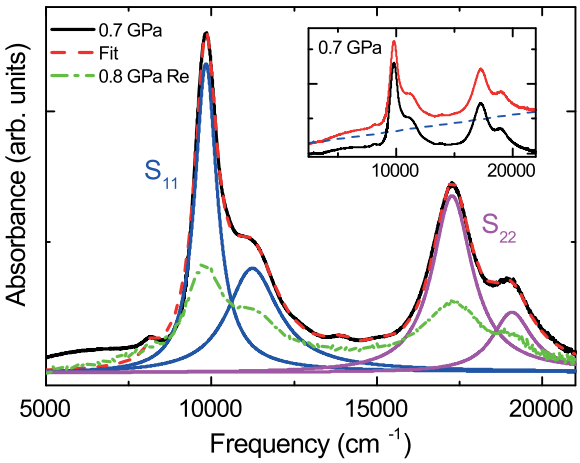

Figure 3 Data evaluation of the absorbance spectra: illustration of the fitting procedure of the spectrum with Lorentzians corresponding to the S_{11} and S_{22} optical transitions. Also, the spectrum at 0.8 GPa after pressure release is plotted. The inset illustrates the subtraction of a linear background (dashed line).

3.2 Optical absorption spectroscopy of a (6,5)-chirality-enriched SWCNT film under pressure

Pressure-dependent absorbance spectra for the (6,5)-CE-SWCNT sample are shown in Fig. 2. Here, a linear background had been subtracted. The background subtraction procedure is illustrated for the lowest pressure value (0.7 GPa) in the inset of Fig. 3. The linear background stems from the tail of the strong π–π^* electronic interband transitions of the graphene sheet centered at around 5 eV. The spectra in Fig. 2 are vertically offset intentionally for better visibility. With increasing pressure one can clearly see a red-shift, broadening, and loss of spectral weight for all absorption bands, in accordance with earlier pressure-dependent optical studies [9, 13, 11]. The red-shift is generally ascribed to σ^*–π^* hybridization and symmetry breaking [26, 33, 34]. Despite the broadening, all optical transitions remain resolved up to the highest pressure of 22 GPa, owing to the high chirality enrichment of the CE-SWCNT sample.

For a quantitative analysis, each background subtracted spectrum was fitted with several Lorentzians, as illustrated in Fig. 3 for the lowest pressure value. As mentioned above, the spectra mainly consist of the S_{11} and S_{22} optical transitions of the (6,5) SWCNTs and some minor contributions of other chiralities. Also shown in Fig. 3 is the spectrum at 0.8 GPa after pressure release, showing the reversibility of the pressure-induced shifts. The reduced intensity of the spectrum after pressure release mostly stems from the fact that the thin film of SWCNTs was torn to small pieces at high pressure ($\approx$ 20 GPa) and thus the total measured area was smaller than in the beginning.

In the following discussion, we only concentrate on the prominent (6,5) peaks of the CE-SWCNT sample because as pointed out in the preceding section they are very sharp and thus more reliable. The relative energy shifts of the optical transition energies of (6,5) SWCNTs, as obtained from the above-explained fitting procedure, are plotted in Fig. 4 as a function of pressure. For comparison, we use the corresponding data of CM-SWCNTs from Anis et al. [13]. They found three anomalies in the pressure-induced shifts at $P_{c1} \approx 3$ GPa, $P_{c2} \approx 7$ GPa and $P_{c3} \approx 13$ GPa and interpreted them in terms of structural phase transitions. We also find an anomaly of the S_{11} transition with an onset at $P_{c1'} \approx 8$ GPa in our data, which we attribute to the structural phase transition where the (6,5) tube is deformed from a circular to an oval shape, in analogy to the case of CM-SWCNTs. This transition is shifted to higher pressures compared to

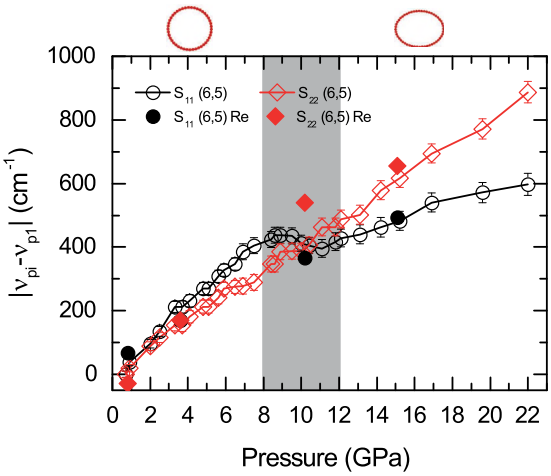

Figure 4 Relative energy shift of the optical transitions as a function of pressure in (6,5)-SWCNTs. The shift was calculated as the difference between the absorption frequency of the contribution ν_{pi} at a pressure p_i, and the absorption frequency ν_{p1} at the lowest pressure value p_1. All the contributions during pressure release are marked as S_{ii} (Re). The shaded gray bar marks the critical pressure regime as discussed in the text. The proposed structural deformation is illustrated on the top.

the CM-SWCNT sample, since the smaller diameter of (6,5) SWCNTs (diameter 0.75 nm) leads to higher mechanical stability. The relative shift of the S_{11} transition continues to rise linearly above $\approx$ 12 GPa. The anomaly at $P_{c1'}$ is not related to the limit of hydrostaticity of the PTM ($\approx$11 GPa [30]), since for the CM-SWCNTs a different behavior is observed despite the same PTM (nitrogen) [13].

Simple elastic theory predicts the collapse pressure of a cylindrical tube to be proportional to d^{-3} [35]. Hasegawa and Nishidate [16] also confirm this relation for isolated SWCNTs using a deformation model based on density-functional theory calculations, not only for the collapse pressure but also for preceding structural deformations. Extrapolating the first critical pressure (i.e., 3 GPa) for CM-SWCNTs with 1.4 nm in diameter to 0.75 nm using the d^{-3} law yields a twofold higher value than the obtained average value of $\approx$ 10 GPa for the observed anomaly for CE-SWCNTs. Elliot et al. [36] and Capaz et al. [15] used molecular dynamics simulations to show that for smaller diameter SWCNTs the dependence of the critical pressure on diameter weakens to rather a $1/d$-dependence, in accordance with our findings. Furthermore, Reich et al. [37] used first-principles calculations and predicted (6,6) SWCNTs (d =0.8 nm) to collapse to an oval shape between 9 and 15 GPa, and Sun et al. [38] also simulated (6,6) SWCNTs using an *ab initio* molecular dynamics method to find a "hard-to-soft" transition at $\approx$ 10 GPa, both of which are in excellent agreement with our value. Similar experimental data have been provided in high pressure-Raman studies. Elliot et al. [36] and Lebedkin et al. [6] studied the $\approx$ 0.8 nm diameter fraction of HiPco-SWCNTs and found critical pressures of 6.6 and $\approx$ 10 GPa, respectively. Deviations from our result could stem from the use of a different PTM, which influences the results quantitatively [39, 40].

Furthermore, the pressure range in which the structural transition occurs, namely from 8 to 12 GPa, appears to be rather large. For a chirality-enriched SWCNT sample, one would expect that the phase transition happens even more abruptly than in chirality-mixed samples, since a possible influence of chirality on the critical pressure would lead to a broadening of the transition for samples with many different chiralities but similar diameters. However, according to Raman spectroscopy data (not shown), the G/D ratio suggests a much higher defect concentration in our CE-SWCNT sample compared to the CM-SWCNT sample [41]. Fagan et al. [42] investigated the influence of radial deformation in combination with vacancies on the electronic properties of SWCNTs. They found that the deformation energy for forming an elliptical cross-section highly depends on the position of the defect. Since the defects are randomly distributed in our sample, this influence of defects on the critical pressure could lead to a broadening of the structural transition as observed in our case. It is also possible that the higher mechanical stability of smaller SWCNTs leads to a broader transition compared to large diameter SWCNTs [43].

Moreover, the S_{22} transition of (6,5) SWCNTs exhibits no anomaly over the whole measured pressure range (see Fig. 4). This is in accordance with theoretical band structure calculations of Charlier et al.[33], indicating that the deformation of nanotubes affects the electronic bands (and hence the optical transitions) in different ways. Liu et al.[34] also showed that the bandstructure in different energy regions is altered differently upon pressure. It was furthermore shown that the pressure-induced band gap changes are highly sensitive to the relative order of certain electronic bands and, thus, can be very different even for SWCNTs with a similar diameter and the same chiral angle [44]. In contrast to the (6,5)-CE-SWCNT sample, in the CM-SWCNT sample with $\approx$ 1.4 nm diameter, all optical transitions show similar behavior in terms of pressure anomalies in their relative shifts [13].

Another difference between the two samples relates to the saturation of the relative shift at high pressures in the case of the CM-SWCNTs, which was interpreted in terms of the collapse of the nanotubes [13]. This saturation is absent in the case of (6,5) SWCNTs. Due to their higher mechanical stability, the collapse pressure might be shifted outside the studied pressure range or, due to their small diameter, a total collapse of the tubes might be inhibited [43, 16].

4 Conclusions In conclusion, we investigated the mechanical stability of a (6,5)-chirality-enriched SWCNT film by optical absorption spectroscopy under pressure. The onset of the first anomaly of the pressure-induced shift of the optical transition S_{11} occurs at $\approx$ 8 GPa in case of (6,5) SWCNTs, in contrast to mixed-chirality SWCNTs with 1.4 nm average diameter, where the first anomaly occurs at $\approx$ 3 GPa. This first anomaly is attributed to a structural phase transition, where the tube's cross-section is deformed from a circular to an oval shape. Thus, the higher value of the critical pressure in the case of (6,5) SWCNTs signals higher mechanical stability due to the smaller tube diameter. Furthermore, a plateau at high pressures, which was earlier attributed to a collapse of SWCNTs, is absent for (6,5) SWCNTs up to a pressure of at least 22 GPa.

Acknowledgements M.K. and C.K. acknowledge financial support by the Deutsche Forschungsgemeinschaft (DFG) through grant no. KU 1432/3-2. W.G. and J.K. acknowledge support from the Basic Energy Sciences (BES) Program of the U.S. Department of Energy (DOE) through grant no. DE-FG02-06ER46308 (for the preparation of SWCNT films) and the Robert A. Welch Foundation through grant no. C-1509 (for SWCNT film characterization).

References

[1] A. Jorio, R. Saito, G. Dresselhaus, and M. S. Dresselhaus, Raman Spectroscopy in Graphene Related Systems (Wiley-VCH Verlag, Weinheim, 2011).

[2] J. Tang, L. C. Qin, T. Sasaki, M. Yudasaka, A. Matsushita, and S. Iijima, Phys. Rev. Lett. **85**, 1887–1889 (2000).

[3] S. M. Sharma, S. Karmakar, S. K. Sikka, P. V. Teredesai, A. K. Sood, A. Govindaraj, and C. N. R. Rao, Phys. Rev. B **63**, 205417 (2001).

[4] A. K. Sood, P. V. Teresdesai, D. V. S. Muthu, R. Sen, A. Govindaraj, and C. N. R. Rao, Phys. Status Solidi B **215**, 393–401 (1999).

[5] S. Reich, H. Jantoljak, and C. Thomsen, Phys. Rev. B **61**, R13389–R13392 (2000).
[6] S. Lebedkin, K. Arnold, O. Kiowski, F. Hennrich, and M. M. Kappes, Phys. Rev. B **73**, 94109 (2006).
[7] C. Caillier, D. Machon, A. San-Miguel, R. Arenal, G. Montagnac, H. Cardon, M. Kalbac, M. Zukalova, and L. Kavan, Phys. Rev. B **77**, 125418 (2008).
[8] A. C. Torres-Dias, S. Cambré, W. Wenseleers, D. Machon, and A. San-Miguel, Carbon **95**, 442–451 (2015).
[9] K. Thirunavukkuarasu, F. Hennrich, K. Kamarás, and C. A. Kuntscher, Phys. Rev. B **81**, 45424 (2010).
[10] B. Anis, F. Börrnert, M. H. Rümmeli, and C. A. Kuntscher, J. Phys. Chem. C **117**, 21995–22001 (2013).
[11] B. Anis, F. Börrnert, M. H. Rümmeli, Kuntscher, and C. A., J. Phys. Chem. C **118**, 27048–27062 (2014).
[12] A. L. Aguiar, E. B. Barros, R. B. Capaz, A. G. S. Filho, P. T. C. Freire, J. M. Filho, D. Machon, C. Caillier, Y. A. Kim, H. Muramatsu, M. Endo, and A. San-Miguel, J. Phys. Chem. C **115**, 5378–5384 (2011).
[13] B. Anis, K. Haubner, F. Börrnert, L. Dunsch, M. H. Rümmeli, and C. A. Kuntscher, Phys. Rev. B **86**, 155454 (2012).
[14] R. S. Alencar, A. L. Aguiar, A. R. Paschoal, P. T. C. Freire, Y. A. Kim, H. Muramatsu, M. Endo, H. Terrones, M. Terrones, A. San-Miguel, M. S. Dresselhaus, and A. G. S. Filho, J. Phys. Chem. C **118**, 8153–8158 (2014).
[15] R. B. Capaz, C. D. Spataru, P. Tangney, M. L. Cohen, and S. G. Louie, Phys. Status Solidi B **241**, 3352 (2004).
[16] M. Hasegawa and K. Nishidate, Phys. Rev. B **74**, 115401 (2006).
[17] T. F. Cerqueira, S. Botti, A. San-Miguel, and M. A. Marques, Carbon **69**, 355–360 (2014).
[18] R. B. Weisman and S. M. Bachilo, Nano Lett. **3**, 1235–1238 (2003).
[19] M. C. Hersam, Nature Nanotechnol. **3**, 387–394 (2008).
[20] M. Kawai, H. Kyakuno, T. Suzuki, T. Igarashi, H. Suzuki, T. Okazaki, H. Kataura, Y. Maniwa, and K. Yanagi, J. Am. Chem. Soc. **134**, 9545–9548 (2012).
[21] H. Liu, D. Nishide, T. Tanaka, and H. Kataura, Nature Commun. **2**, 309 (2011).
[22] X. Tu, S. Manohar, A. Jagota, and M. Zheng, Nature **460**, 250–253 (2009).
[23] F. Yang, X. Wang, D. Zhang, J. Yang, Luoda, Z. Xu, J. Wei, J. Q. Wang, Z. Xu, F. Peng, X. Li, R. Li, Y. Li, M. Li, X. Bai, F. Ding, and Y. Li, Nature **510**, 522–524 (2014).
[24] J. A. Fagan, C. Y. Khripin, C. A. Silvera Batista, J. R. Simpson, E. H. Hároz, A. R. Hight Walker, and M. Zheng, Adv. Mater. **26**, 2800–2804 (2014).
[25] X. He, W. Gao, L. Xie, B. Li, Q. Zhang, S. Lei, J. M. Robinson, E. H. Hároz, S. K. Doorn, W. Wang, R. Vajtai, P. M. Ajayan, W. W. Adams, R. H. Hauge, and J. Kono, Nature Nanotechnol. **11**, 633–638 (2016).
[26] Z. Wu, Z. Chen, X. Du, J. M. Logan, J. Sippel, M. Nikolou, K. Kamaras, J. R. Reynolds, D. B. Tanner, A. F. Hebard, and A. G. Rinzler, Science **305**, 1273–1276 (2004).
[27] W. Wenseleers, S. Cambré, J. Čulin, A. Bouwen, and E. Goovaerts, Adv. Mater. **19**, 2274–2278 (2007).
[28] G. Huber, K. Syassen, and W. B. Holzapfel, Phys. Rev. B **15**, 5123–5128 (1977).
[29] H. K. Mao, J. Xu, and P. M. Bell, J. Geophys. Res.: Solid Earth **91**, 4673–4676 (1986).
[30] S. Klotz, J. C. Chervin, P. Munsch, and G. Le Marchand, J. Phys. D: Appl. Phys. **42**, 75413 (2009).
[31] R. Saito, G. Dresselhaus, and M. S. Dresselhaus, Phys. Rev. B **61**, 2981–2990 (2000).
[32] H. Kataura, Y. Kumazawa, Y. Maniwa, I. Umezu, S. Suzuki, Y. Ohtsuka, and Y. Achiba, Synth. Met. **103**, 2555–2558 (1999).
[33] J. C. Charlier, P. Lambin, and T. W. Ebbesen, Phys. Rev. B **54**, R8377–R8380 (1996).
[34] G. Liu, X. Wang, J. Chen, and H. Lu, Phys. Status Solidi B **245**, 689–694 (2008).
[35] M. Levy, J. Math. Ser. **3**, 7 (1884).
[36] J. A. Elliott, J. K. W. Sandler, A. H. Windle, R. J. Young, and M. S. P. Shaffer, Phys. Rev. Lett. **92**, 95501 (2004).
[37] S. Reich, C. Thomsen, and P. Ordejón, Phys. Status Solidi B **235**, 354–359 (2003).
[38] D. Y. Sun, D. J. Shu, M. Ji, F. Liu, M. Wang, and X. G. Gong, Phys. Rev. B **70**, 165417 (2004).
[39] C. A. Kuntscher, A. Abouelsayed, K. Thirunavukkuarasu, and F. Hennrich, Phys. Status Solidi B **247**, 2789–2792 (2010).
[40] B. Anis, F. Börrnert, M. H. Rümmeli, and C. A. Kuntscher, Phys. Status Solidi B **250**, 2616–2621 (2013).
[41] Y. Miyata, K. Mizuno, and H. Kataura, J. Nanomater. **2011**, 18:1–18:7 (2011).
[42] S. B. Fagan, L. B. da Silva, and R. Mota, Nano Lett. **3**, 289–291 (2003).
[43] S. P. Chan, W. L. Yim, X. G. Gong, and Z. F. Liu, Phys. Rev. B **68**, 75404 (2003).
[44] O. Gülseren, T. Yildirim, S. Ciraci, and C. Kilic, Phys. Rev. B **65**, 155410 (2002).